COBEM 2021 Florianópolis - Brasil
26th ABCM International Congress of Mechanical Engineering
November 22-26, 2021. Florianópolis, SC, Brazil

COB-2021-0914
STATIC EQUILIBRIUM ANALYSIS OF A DISTRIBUTION LINE RIDING ROBOT WITH ACTIVE BALANCING SYSTEM

João Vitor Fernandes de Brito
Estevan Hideki Murai
Gustavo Queiroz Fernandes
Rogério Augusto Antunes Pereira
Daniel Martins
Federal University of Santa Catarina. Campus Universitário Reitor João David Ferreira Lima, s/nº - Trindade, Florianópolis – SC, 88040-900
joaov.brito92@gmail.com
estevan.murai@ufsc.br
gustavo.fernandes@posgrad.ufsc.br
rogerio.antunes@posgrad.ufsc.br
daniel.martins@ufsc.br

Roberto Kinceler
Alessandro Pedro Dadam
Centrais Elétricas de Santa Catarina S.A. Av. Itamarati, 160 - Itacorubi, Florianópolis - SC, 88034-900
rkinceler@celesc.com.br
alessandropd@celesc.com.br

Abstract. *In the power distribution field, energy key performance indicators are important indexes for measuring a company competitiveness and the provided energy quality. Preventive and corrective maintenances are crucial to avoid power outages. Using an automated inspection system can result in faster and more precise inspections. However, designing a distribution line inspection robot presents several challenges. One issue is the robot stability. For effectiveness and safety reasons, the robot must remain stable when moving along the cable or transposing obstacles. In this paper, the static equilibrium analysis of a distribution line riding robot with active balancing system is done. This is a preliminary study to assess the feasibility of an actuated equilibrium system for the robot under development. Initially, the geometrical limitations of distribution lines are presented. Then, the distribution line riding robot is briefly described. The static equilibrium equations are presented and implemented in Matlab. The analysis is carried out considering the robot mass and two movable counterweight masses. The distribution line components are also taken into account. Thus, the constraints imposed by space limitations and insulators geometry are analyzed. The analysis indicates that the proposed active balancing system has limited effectiveness and other design decisions, such as lowering the center of mass, have higher impact on robot stability. Therefore, other balancing methods, such as passive balancing systems, may be promising.*

Keywords: *static equilibrium analysis, distribution line inspection robot, active balancing system, robot stability analysis.*

1. INTRODUCTION

The economic development and growth of urban centers have caused an increase in the demand and consumption of electricity, requiring an important network for its transmission and distribution (Gonçalves and Carvalho, 2014). At the same time, to guarantee the safety, reliability and quality of the power supply, it is essential to carry out periodic inspections to identify and repair defects in the line components, such as cables and insulators. Besides inspection, it is also important to clean the line components at a regular basis. To operate in close proximity or in contact with live-lines poses a constant risk of falling from great heights as well as electrical shocks. Besides the risks, distribution line maintenance requires high level of both cognitive functions and physical workload. As maintenance is a specialized job, it requires training and refresher courses. Thus, obtaining qualified professionals is difficult and expensive. The solution to some risks would be to carry out maintenance on de-energized lines, but it would also create other problems with a society that requires a service without interruption in the supply of electricity (Parker and Draper, 1998).

The inspection and maintenance of transmission and distribution lines can be carried out by a professional working on the ground or with the aid of equipment. However, human inspections have disadvantages, such as long inspection cycle,

high labor intensity, high expense and high danger (Wang *et al.*, 2010). Furthermore, they are subject to misinterpretation and misdiagnosis, sometimes leading to inappropriate maintenance actions. The use of equipment such as helicopters and unmanned aerial vehicles (UAVs) makes the inspection process faster and more efficient, but aerial inspection is expensive and there is always the risk of contact with live-lines and death.

The use of helicopters for inspection is more efficient than manual operation, but it is costly and climate-dependent (Wang *et al.*, 2010), requiring operators with advanced technical capacity and high level of training. In addition, they present high operational risks, having already been registered accidents with fatal victims during the execution of inspection services (Homma *et al.*, 2017). Hrabar *et al.* (2010) present the development of an autonomous helicopter for aerial inspection of transmission lines. One difficulty pointed out is the precise control of the aircraft required to avoid vibrations, which impairs the focus of the image capture system.

The use of UAVs is very similar to automated inspection of helicopters, sharing some common problems such as camera stabilization, pole tracking and automatic defect detection (Luque-Vega *et al.*, 2014). The basic principle of UAVs is to carry out visual inspections while flying close to the power grid (Elizondo *et al.*, 2010). Therefore, the use of such equipment does not allow maintenance operations due to the difficulty of installing a robotic arm or repair device on the UAV. Another problem in using UAVs is government regulations, as they are different for each country. In Brazil, the autonomous operation of aircraft is prohibited by resolution E94.103(c) "General rules for the operation of unmanned aircraft" of the National Civil Aviation Agency (ANAC, 2017).

In view of this, many theoretical and experimental studies have been carried out with the aim of developing autonomous machines that move on the cable to perform inspections and/or repairs (Katrasnik *et al.*, 2010; Miller *et al.*, 2017; Jalal *et al.*, 2013; Toussaint *et al.*, 2009; Aracil *et al.*, 2002; Hydro-Québec, 2018; IEEE, 2010). The development of an inspection robot is a complex task due to the variability of elements present in the electrical network, such as insulators, suspended switches, fuses, cross arms and even Rufous Hornero nests, which can act as obstacles for the robot. Furthermore, there are still challenges related to stability, controllability, power supply, autonomy and insulation.

One approach found in the literature to overcome obstacles is the addition of more degrees of freedom in the robot. However, more degrees of freedom mean a greater number of parts and actuators, increasing the robot mass and volume. Mass is an important design requirement as the robot cannot exceed the load capacity of the distribution line, particularly the cables strength. As for the volume, the robot may have contact with two different points on the line at the same time and, depending on the materials used, this double contact can cause short circuits and further accidents. Additionally, more degrees of freedom may also require more reliable electronics and control systems to keep the robot stable on the cable. These additional components increase the robot costs, which may affect the robot economic viability.

In this context, a partnership between the Electric Power Plants of Santa Catarina (Celesc) and the Laboratory of Applied Robotics (LAR) of the Federal University of Santa Catarina (UFSC), designed an inspection robot capable of moving and overcoming obstacles in distribution lines. This article evaluates the static balance capability of a robot mounted on a distribution line with an active balancing system. It is worth noting that this is a preliminary analysis to assess the feasibility of an active balancing system for the robot being developed. A deeper understanding of the robot behaviour during obstacle transposition would require to carry out a dynamic analysis. For instance, when the contact between robot and obstacle occurs, higher transposition velocities could cause the robot to oscillate, to lose contact with the distribution line and even to jump over the obstacles. Additionally, the sliding of any of the movable masses would result in changes in the robot angular momentum, possibly affecting the robot equilibrium capacity. Initially, in Section 2, the geometric delimitation of the distribution lines is presented. In Section 3 the robot is briefly described, as well as the stability maps for each situation considered, relating different contact points along the wheel to a maximum stability inclination angle. Then, in Section 4, the analysis is performed considering the robot mass and a mobile counterweight mass. Finally, the results are presented in Section 5, as well as a discussion on the feasibility of using active balancing systems for distribution line inspection robots. The conclusions are presented in Section 6.

2. GEOMETRICAL DELIMITATION IN DISTRIBUTION LINES

Before designing a robot for distribution line inspection, it is necessary to identify the geometric delimitation imposed by distribution lines. To do so, a distribution line was selected as a model line for the robot design. In this section, this model line is described.

The model line is a 13.8kV distribution line, located in Florianópolis, Brazil. The model line begins on Deputado Antônio Edu Vieira street, running along João Pio Duarte Silva street until Maestro Aldo Krieger street. Then, the line continues on Maestro Aldo Krieger street until Trindade substation. The greatest terrain slope on the model line is 5,56°. The greatest azimuth on the model line is 136° (at an insulator, the line deviates 44° laterally from a straight line reference.

The geometric delimitation is determined by the cross arms components, their geometries and dimensions. The model line presents two levels of distribution lines, one on top of the other. Thus, two possibilities are taken into account: placing the robot on the lower line or on the upper line. As expected, the lower line presents more geometric delimitation.

The insulator varies from cross arm to cross arm. Two types of insulators present critical dimensions: pin-type insulators, with 230 mm diameter and 215 mm height; and line post insulators, with 124 mm diameter and 305 mm

height.

The insulators position were estimated using images taken from three points of view for each cross arm along the model line. Then, the exact position was determined using the cross arm hole pattern (Celesc, 2001) together with the cross arm assembly manual (Celesc, 2014). Two scenarios that presented a more constrained region were identified and considered as critical cases.

In the first critical case, the shortest distance between insulators center is 500 mm. The shortest distance between insulators body is 270 mm. The shortest height between two cross arms on the same pole is 831 mm. The dimensions are shown in Fig. 1, as well as the obstacle free region (shaded area).

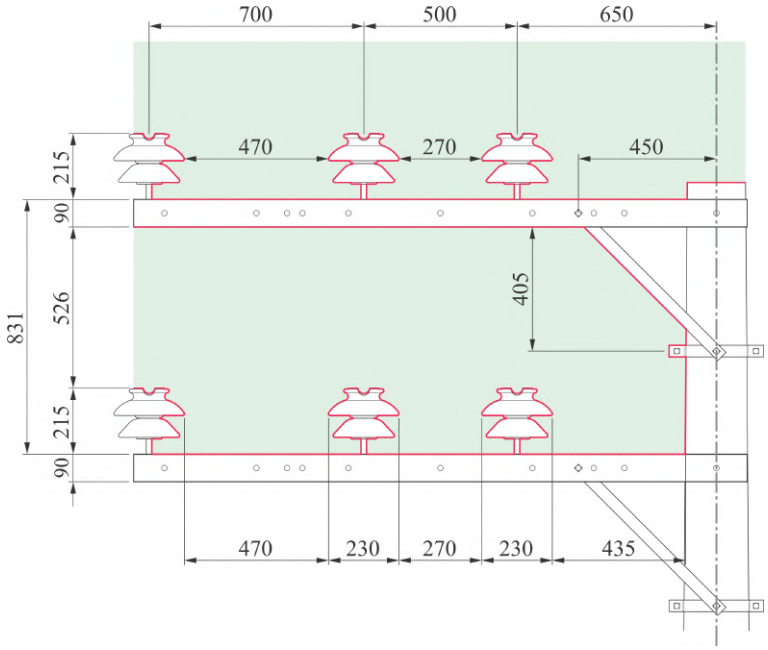

Figure 1. Geometrical delimitation - case 1.

In the second critical case, the shortest distance between insulators center is 600 mm. The shortest distance between insulators body is 476 mm. In this case, the height between two cross arms on the same pole is 915 mm. However, as the insulator used is taller than the insulator in case 1, the available space between the upper cross arm and the top of the lower cross arm insulator is 520 mm. The dimensions are shown in Fig. 2, as well as the obstacle free region (shaded area).

3. ROBOT DESIGN

The robot considered in this study is composed of a wheel and an outer structure. The wheel profile is composed by two arcs with opposite concavities. This geometry was developed to center the robot on the aluminium conductors and on the obstacles (Fig. 3). The outer structure remains suspended as the wheel rotates along the cable. In addition, most of robot mass corresponds to structural components, electromagnetic shield, batteries, sensors and other electronic components, which are located at both ends of the outer structure. This mass distribution yields a center of mass below the contact between wheel and cable. Therefore, by analyzing the frontal view shown in Fig. 3, when the robot presents an angular displacement (α) to any side, the center of mass creates a moment (M_{RP}) at the rotation point that maintains the system stable.

However, the critical operating conditions are when the robot transposes obstacles. During transpositions, the contact between wheel and distribution line is not necessarily centered along the robot structure. This misalignment causes an angular displacement in robot axis (Fig. 4). Depending on the center of mass location in relation to the contact point, the moment at the rotation point can restore the robot horizontal alignment (a) or contribute for the rotation to continue (b).

One possible solution found by the authors to reduce the trend of falling shown in Fig. 4 and to improve stability was to consider the outer structure masses as active balancing systems that laterally translates in order to move the overall center of mass. According to Fig. 5, for purpose of simplifying the analyses, the center of masses of the left movable mass (CM_{LM}) and the right movable mass (CM_{RM}) are measured separately from the main body's center of mass (CM_{MB}). The three center of masses account for a total of 15 kg and their positions are described using the coordinate system located at the original point of contact between wheel and cable (see Fig. 5).

As described in Section 2, the distribution line geometry imposes constraints on the robot maximum mass and dimensions. Active counterbalancing systems require more mass and reduce the robot autonomy. For instance, gyroscopes

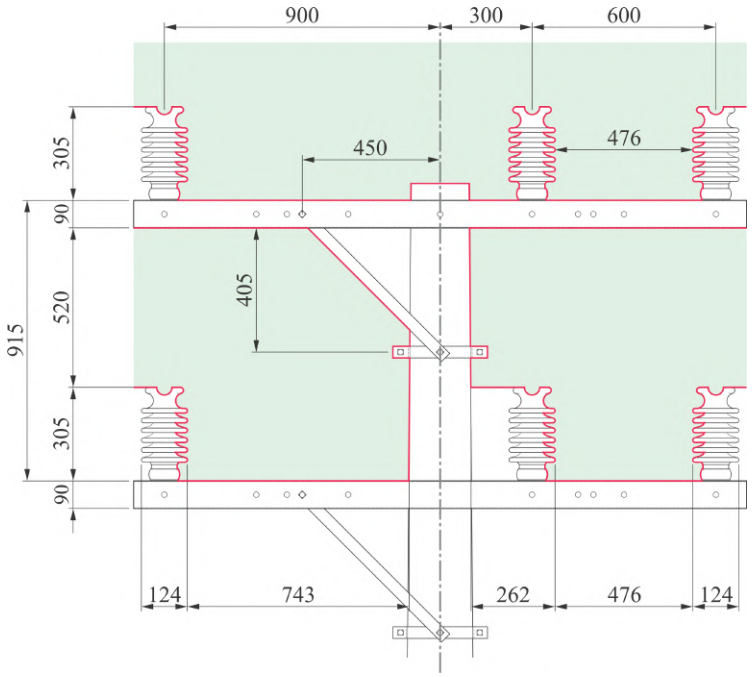

Figure 2. Geometrical delimitation - case 2.

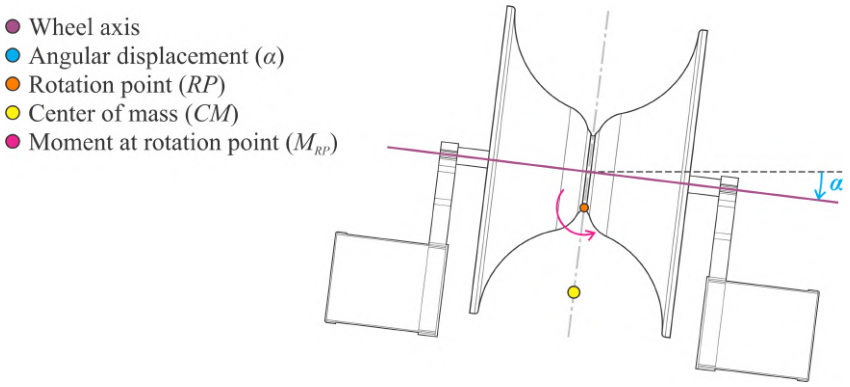

Figure 3. Designed robot moving along the cable.

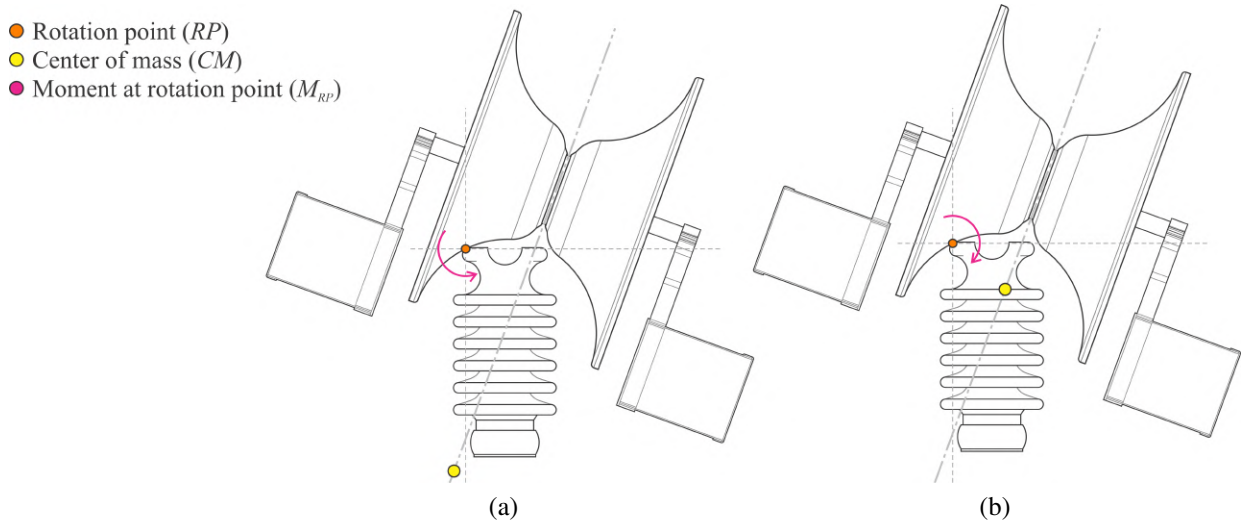

Figure 4. Designed robot transposing an insulator in (a) stable and (b) unstable conditions.

add mass located at a considerable distance from the spinning axes and rotate at high speed. Thus, this approach would increase the robot total mass by adding flying wheels, motors and support structures. The robot total mass could surpass

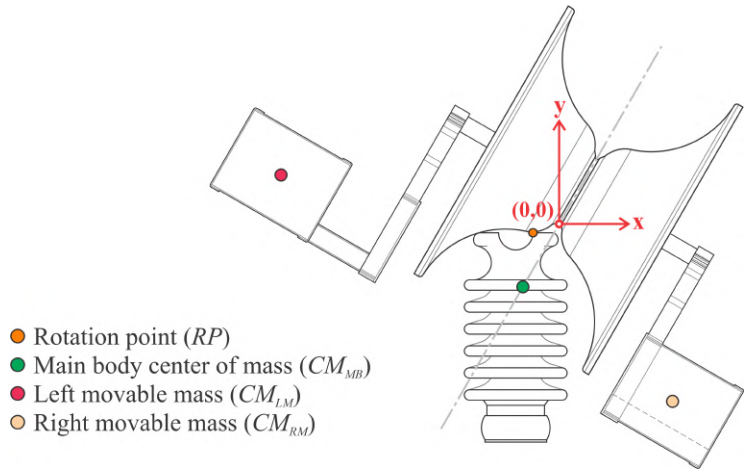

Figure 5. Designed robot with the movable masses actuated in order to keep the system stable.

the limit of 15 kg, which was considered as the maximum load admissible on the aluminium wire. In distribution lines, most obstacles are located below the power line. Adding a gyroscope at such space could result in hitting obstacles or undesired short circuits. Adding a gyroscope above the power line raises the robot center of mass. Besides that, as the gyroscope needs to be working at all times, even when the robot is standing still, the robot autonomy is reduced.

Figure 6 shows the designed robot size in relation to the distribution line when the robot is approaching the insulator. Figure 6a shows the distance between the outer structure and the cross arm. This distance is critical because a contact between outer structure and cross arm creates a moment around the vertical axis which results in misalignment. Figure 6b shows the robot over the insulator, with the shortest distance between the robot and the lateral line insulator indicated. In Fig. 6b, the energy grid is represented according to the scenario illustrated in Fig. 2, as it was more frequently observed in the model line. The insulators presented are the pin-type once they have higher diameter and reduce the active equilibrium system feasible space.

The distances in Fig. 6 impose geometrical constraints to the outer structure position. Besides that, the wheel profile also plays an important role. The smaller the wheel diameter, the lower the robot center of gravity but the closer the outer structure is to the cross arm. On the other hand, placing the outer structure closer to the wheel axis increases the distance between the outer structure and the cross arm, but it also raises the robot center of mass. Finally, the outer structure width and length are limited by the distances in Fig. 6, which constrains how much mass can be placed at the outer structure lowest point.

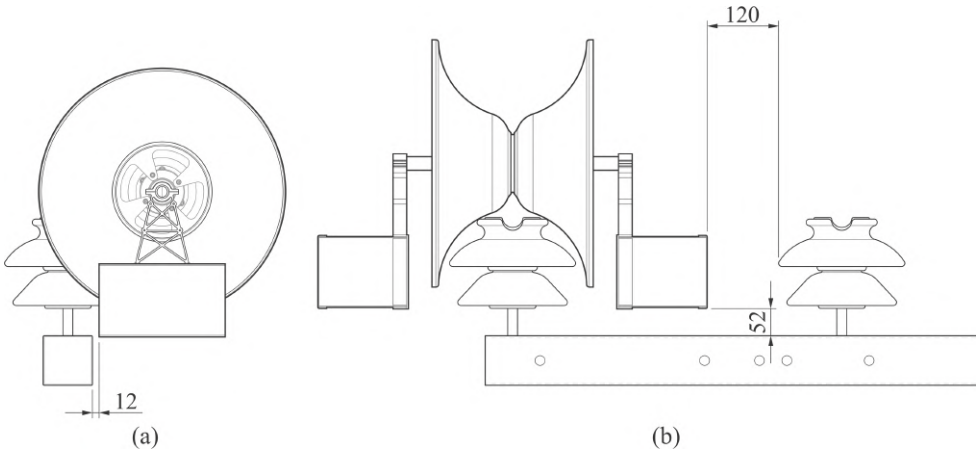

Figure 6. Some of robot dimension constraints when transposing obstacles, the movable masses are in retracted position.

The next sections present the mathematical formulation for the static stability study and a collision analysis for the proposed balancing system.

4. ACTIVE EQUILIBRIUM ANALYSIS

This static equilibrium analysis consists on the equilibrium of moment evaluation for the robot frontal plane. This evaluation takes into account the moment generated by the main body weight, left movable weight and right movable weight around a rotation point, Fig. 5. The following considerations are taken for this analysis:

1. It is applied a clockwise angular displacement (α) to the wheel axis of the robotic system, see Fig. 3. Due to this angular displacement, the contact between the wheel and the insulator is limited to a single rotation point (RP).
2. The main body center of mass ($\mathbf{CM_{MB}}$) is located on the y axis of the initial coordinated system. The movable centers of mass ($\mathbf{CM_{LM}}$ and $\mathbf{CM_{RM}}$) are in their retracted positions and symmetrically placed in relation to the initial coordinate system. The movable centers of mass positions are fixed through the analysis according to the values presented in the initial coordinated system (Fig. 7). These coordinates are also shown in Table 1.
3. The total movable mass of the system is equally distributed between the right and left movable masses.
4. In order to evaluate the worst case scenarios, where the main body center of mass ($\mathbf{CM_{MB}}$) may tend to increase the angular displacement of the robot, the rotation point (RP) is limited to the left side of the wheel in this analysis.
5. The relative position between the robot and insulator is defined by two independent variables: the position of the rotation point (RP) along the wheel left curvature and the clockwise angular displacement applied to the robot (α).

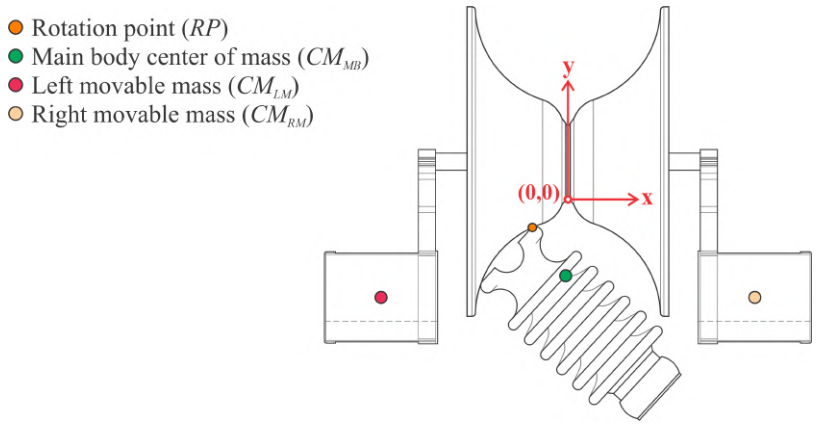

Figure 7. Initial coordinate system.

Table 1. Main body and movable masses center of mass initial coordinates.

Element	Coordinate x [mm]	Coordinate y [mm]
Main body center of mass ($\mathbf{CM_{MB}}$)	0	Variable
Left movable mass ($\mathbf{CM_{LM}}$)	-365	-210
Right movable mass ($\mathbf{CM_{RM}}$)	365	-210

The first step of this analysis is to update the position of every point due to the angular displacement applied to the robotic system, Fig. 8. For the left movable center of mass ($\mathbf{CM_{LM}}$) it is also necessary to add the horizontal displacement (Δ_x) applied to its initial horizontal coordinate. The updated position of the rotation point ($\mathbf{RP'}$), main body center of mass ($\mathbf{CM'_{MB}}$), left movable center of mass ($\mathbf{CM'_{LM}}$) and right movable center of mass ($\mathbf{CM'_{RM}}$) are defined by the following equations.

$$\mathbf{RP'} = \left[|\mathbf{RP}|.cos\left(atg\left(\frac{RP_y}{RP_x}\right) - \alpha\right), |\mathbf{RP}|.sin\left(atg\left(\frac{RP_y}{RP_x}\right) - \alpha\right), 0\right] \tag{1}$$

$$\mathbf{CM'_{MB}} = \left[|\mathbf{CM_{MB}}|.cos\left(atg\left(\frac{CM_{MBy}}{CM_{MBx}}\right) - \alpha\right), |\mathbf{CM_{MB}}|.sin\left(atg\left(\frac{CM_{MBy}}{CM_{MBx}}\right) - \alpha\right), 0\right] \tag{2}$$

$$\begin{aligned}\mathbf{CM'_{LM}} = \Bigg[&|\mathbf{CM_{LM}} + \Delta_x|.cos\left(atg\left(\frac{CM_{LMy}}{CM_{LMx} + \Delta_x}\right) - \alpha\right), \\ &|\mathbf{CM_{LM}} + \Delta_x|.sin\left(atg\left(\frac{CM_{LMy}}{CM_{LMx} + \Delta_x}\right) - \alpha\right), 0\Bigg]\end{aligned} \tag{3}$$

$$\mathbf{CM'_{RM}} = \left[|\mathbf{CM_{RM}}|.cos\left(atg\left(\frac{CM_{RMy}}{CM_{RMx}}\right) - \alpha\right), |\mathbf{CM_{RM}}|.sin\left(atg\left(\frac{CM_{RMy}}{CM_{RMx}}\right) - \alpha\right), 0\right] \tag{4}$$

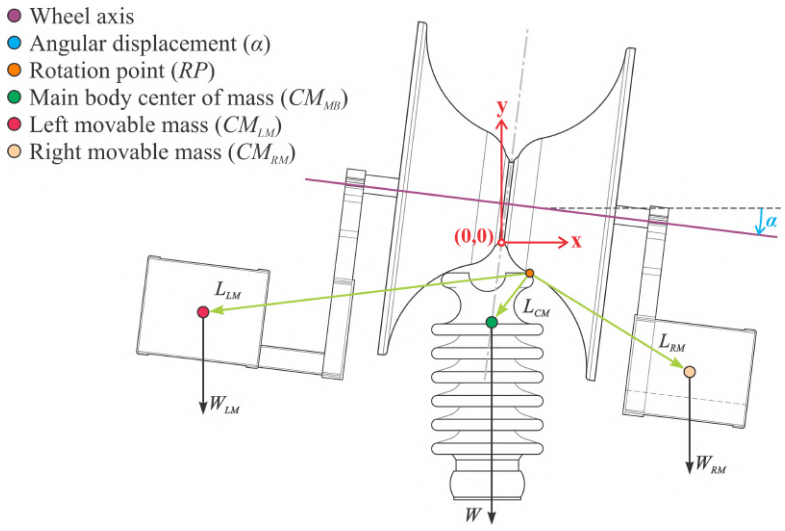

Figure 8. Updated coordinate system.

Once each point is updated, the position of each center of mass in relation to the rotation point ($\mathbf{RP}'$) is evaluated, Eq. 5 to 7. Each center of mass has a weight vector ($\mathbf{W}$) parallel to the updated vertical axis, Fig. 8. The moment applied by each mass is obtained by the cross products of their relative position vector and weight vector (Hibbeler, 2017). Since the weight vectors are unidirectional, the moment applied by each mass can be simplified as Eq. 8 to 10 show.

$$\mathbf{L_{MB}} = [L_{MBx}, L_{MBy}, 0] = \mathbf{CM'_{MB}} - \mathbf{RP'} \tag{5}$$

$$\mathbf{L_{LM}} = [L_{LMx}, L_{LMy}, 0] = \mathbf{CM'_{LM}} - \mathbf{RP'} \tag{6}$$

$$\mathbf{L_{RM}} = [L_{RMx}, L_{RMy}, 0] = \mathbf{CM'_{RM}} - \mathbf{RP'} \tag{7}$$

$$\mathbf{M_{MB}} = [M_{MBx}, M_{MBy}, M_{MBz}] = \mathbf{L_{MB}} \times \mathbf{W}_{MB} \rightarrow M_{MBz} = -|\mathbf{W_{MB}}|.L_{MBx} \tag{8}$$

$$\mathbf{M_{LM}} = [M_{LMx}, M_{LMy}, M_{LMz}] = \mathbf{L_{LM}} \times \mathbf{W}_{LM} \rightarrow M_{LMz} = -|\mathbf{W_{LM}}|.L_{LMx} \tag{9}$$

$$\mathbf{M_{RM}} = [M_{RMx}, M_{RMy}, M_{RMz}] = \mathbf{L_{RM}} \times \mathbf{W}_{RM} \rightarrow M_{RMz} = -|\mathbf{W_{RM}}|.L_{RMx} \tag{10}$$

The sum of these moments represents the moment of the robot around the rotation point (M_{RP}). If this moment presents a positive value the robotic system will gradually return to the horizontal position, otherwise the angular displacement will increase, which may eventually cause the fall of the robot.

$$M_{RP} = M_{MBz} + M_{LMz} + M_{RMz} \tag{11}$$

A code was developed to evaluate the capability of this counterbalancing system. This code computed the moment (M_{RP}) for a set of angular displacement and main body mass configurations. The code inputs are listed as follows.

- The rotation point initial position.
- The main body center of mass initial vertical position.
- Total mass value.
- Angular displacement applied to the robotic system.

The following section is dedicated to discuss some of the results obtained.

5. RESULTS AND DISCUSSIONS

The output of the developed code is a three-dimensional graph in which the first axis is the moment (M_{RP}), the second axis is the main body mass (m_{MB}) and the third axis is the applied horizontal displacement (Δ_x), Fig. 9. The graphs take the shape of a three-dimensional surface. To facilitate the interpretation and comparison, the results are presented for a fixed angular displacement of 45° in a two-dimensional view with a color scheme to identify the value of the moment (M_{RP}), Fig. 10 to 12. The transition between cyan and yellow indicates configurations which the moment (M_{RP}) will be close to zero, thus the robotic system may maintain the current applied angular displacement (close to stability). The dark red color represents a configuration which the moment (M_{RP}) will be negative, which will tend to increase the clockwise angular displacement, therefore further decreasing the moment (M_{RP})(unstable). The dark blue color indicates a configuration which the moment (M_{RP}) will be positive, which will tend to reduce the clockwise angular displacement, therefore decreasing the moment (M_{RP}), approaching stability.

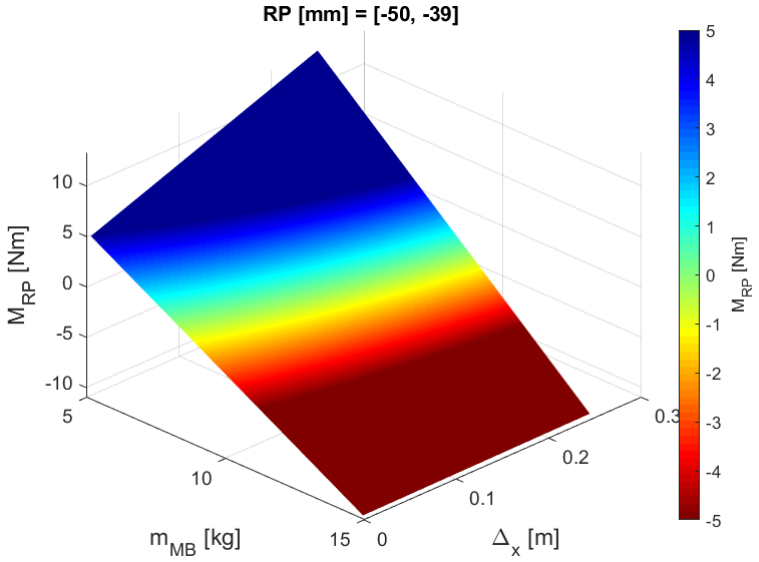

Figure 9. Output graph from the code.

Analyzing Eqs. 1 to 11, the moment increases with:

- Decrease of the vertical initial position of the main body center of mass, CM_{MBy}.
- Reduction of the distance from the initial rotation point to the origin, $|\mathbf{RP}|$.
- Reduction of the main body mass, m_{MB}.
- Increase of the horizontal displacement, Δ_x.

These behaviours can be seen through Fig. 10, 11 and 12. It is also visible that because of the geometrical delimitation, for the same $\mathbf{RP}$, the variation of the $\mathbf{CM_{MB}}$ is more relevant to the resulting moment than the variation of the horizontal displacement (Δ_x). This means the active balancing system proposed is a less effective approach to achieve stability than lowering the main body center of mass.

Additionally, a preliminary structural analysis was done. This analysis showed a main body mass of 10 kg. However, as Figs. 10-12 show, a robot with $m_{MB} = 10$ kg presents a limited effectiveness for this active balancing system.

6. CONCLUSIONS

In this study, the static equilibrium analysis of a distribution line riding robot with active balancing system was carried out. The analysis was performed considering the robot mass and two movable counterweight masses. The use of an active balancing system based on lateral mass displacements presents a limited effectiveness due mass distribution and geometrical limitations. Other active systems, such as gyroscopes, were disregarded as valid solution principles due to their mass, size and energy consumption. As the analysis showed, lowering the main body center of mass is critical to increase the robot stability.

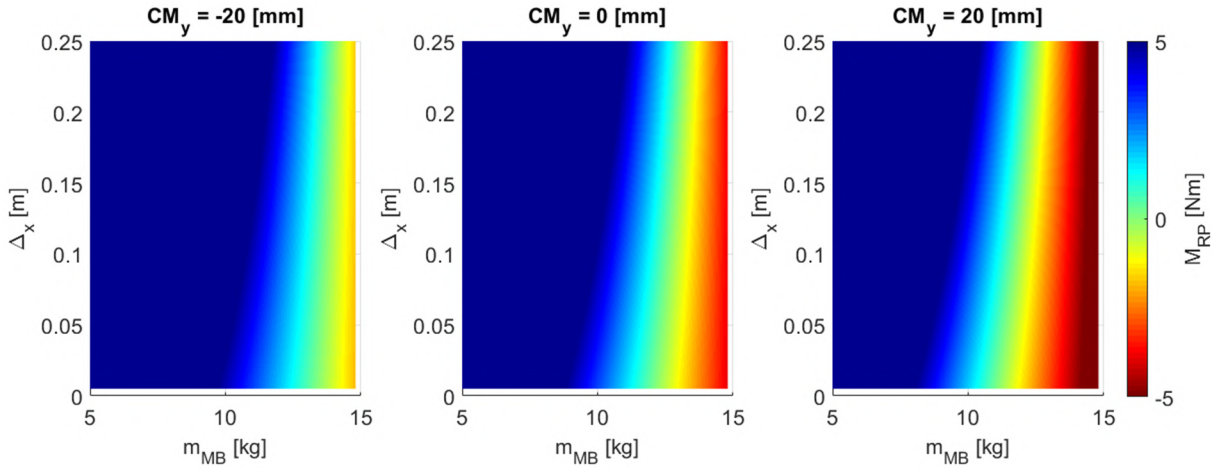

Figure 10. Output graphs for $RP[mm] = [-20, -20]$.

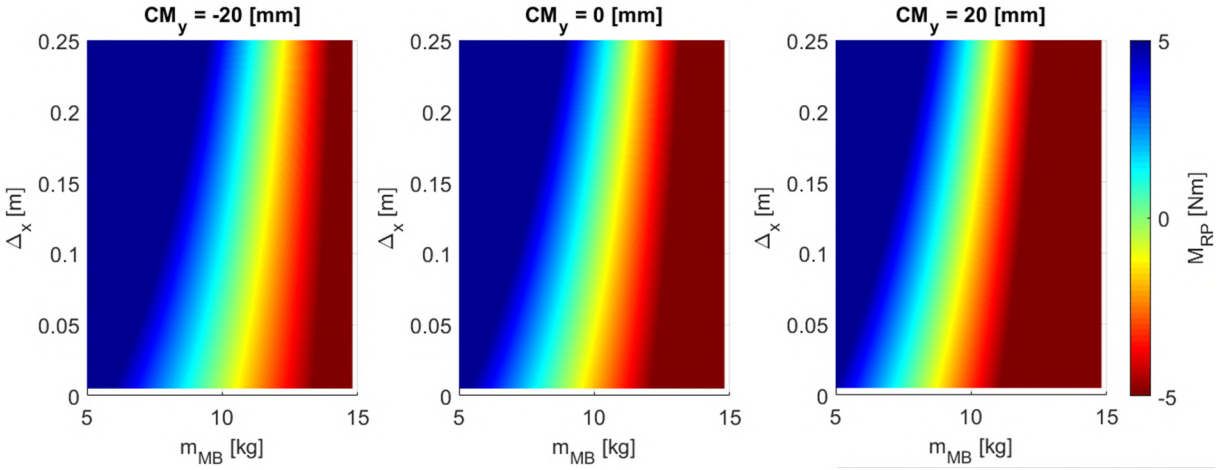

Figure 11. Output graphs for $RP[mm] = [-50, -38, 6]$.

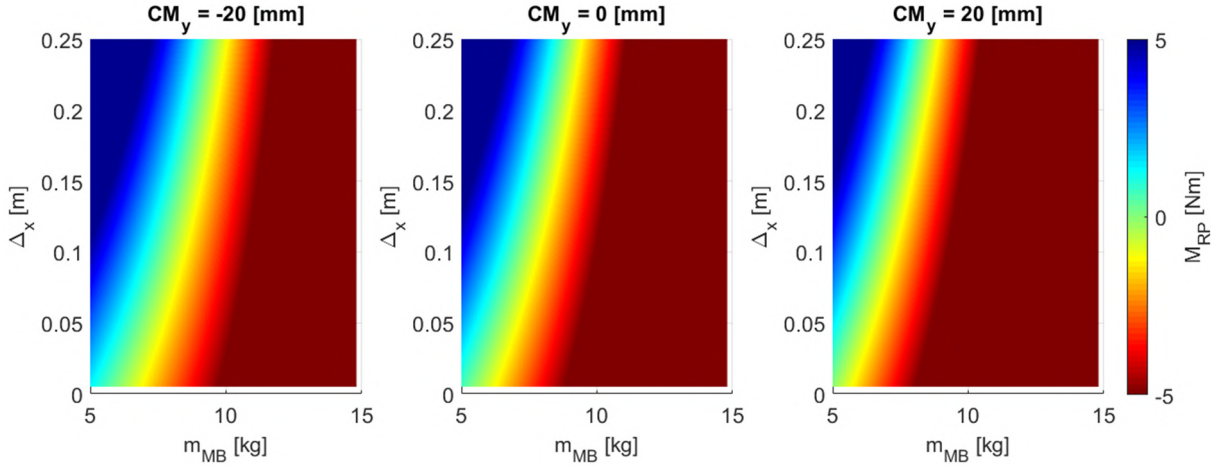

Figure 12. Output graphs for $RP[mm] = [-80, -55, 1]$.

A code was developed to map the sum of moments as a function of the fixed mass and the absolute displacement of the movable mass. Through these mappings, it was observed that the vertical position of the $\mathbf{CM_{MB}}$ has a great influence due to its high mass and the possibility of changing quadrants; in addition, the $\mathbf{CM_{MB}}$ above the point of contact with the cable (y>0) makes it difficult to balance the system. It is also added that the variation of the maximum displacement of the movable mass ($\Delta_{x\ max} = 120$ mm) is limited by the chassis width, distance between insulators and/or distance in relation to the cross arm. This study is an initial analysis of the feasibility of using an active balancing system, and

the static analysis was performed only considering the moment around the z-axis. However, as the use of an equilibrium system based on active balancing was not promising, other alternatives will be studied.

7. ACKNOWLEDGEMENTS

This work was made as part of the R&D project entitled "Development of a Robotized System for Inspection of Electricity Distribution Lines" (05697-0317 / 2017), regulated by ANEEL and financed by Centrais Elétricas de Santa Catarina (Celesc). The project is executed at the Laboratory of Applied Robotics (LAR), at UFSC, and financially managed by FEESC. The authors also thank CNPq and CAPES for the financial support.

8. REFERENCES

ANAC, 2017. "General requirements for unmanned aircraft of civilian use". Agência Nacional de Aviação Civil - ANAC, Brasília, https://www.anac.gov.br/en/drones/files/rbac-e-no-94-amdt-00-english.pdf. Accessed 12 June 2021.

Aracil, R., Ferre, M., Hernando, M. and Sebastian, J.M., 2002. "Telerobotic system for live-power line maintenance: Robtet". *Control Engineering Practice*, Vol. 10, No. 11, pp. 1271–1281.

Celesc, 2001. "E-313.0022: Cruzetas de concreto armado".

Celesc, 2014. "E-313.0002: Estruturas para redes aéreas convêncionais de distribuição".

Elizondo, D., Gentile, T., Candia, H. and Bell, G., 2010. "Ground based robots for energized transmission line work-technology description, field projects and technical-economical justification of their application". In *2010 IEEE/PES Transmission and Distribution Conference and Exposition: Latin America (T D-LA)*. pp. 700–705. doi:10.1109/TDC-LA.2010.5762960.

Gonçalves, R.S. and Carvalho, J.C.M., 2014. "A mobile robot to be applied in high-voltage power lines". *Journal of the Brazilian Society of Mechanical Sciences and Engineering*, Vol. 37, pp. 349–359. doi:10.1007/s40430-014-0152-0.

Hibbeler, R., 2017. *Estática: mecânica para engenharia*. Pearson Education do Brasil. ISBN 9788543016245.

Homma, R.Z., Filho, L.A.P.A., Cosentino, A., Szymanski, C., Kinceler, R., Roder, B.B., Smiderle, C.D., Oliveira, P.C., Trentin, R.G. and Ferro, H.F., 2017. "Inspeção autônoma em linhas aéreas de transmissão e distribuição – metodologia para aquisição, tratamento, armazenagem e análise de imagens obtidas por aeronaves remotamente pilotadas (arp)". João Pessoa, Brazil.

Hrabar, S., Merz, T. and Frousheger, D., 2010. "Development of an autonomous helicopter for aerial powerline inspections". In *The 1st International Conference on Applied Robotics for the Power Industry*. pp. 1–6. doi: 10.1109/CARPI.2010.5624432. URL `https://eprints.qut.edu.au/40822/`.

Hydro-Québec, 2018. "Lineranger: A revolution in transmission line robotics". Hydro-Québec, http://www.hydroquebec.com/robots/en/. Accessed 28 August 2018.

IEEE, 2010. "Expliner". IEEE, ROBOTS your guide to the world of robotics, https://robots.ieee.org/robots/expliner/. Accessed 16 June 2021.

Jalal, M.F.A., Sahari, K., Anuar, A., Arshad, A.D.M. and Idris, M.S., 2013. "Conceptual design for transmission line inspection robot". Earth and Environmental Science.

Katrasnik, J., Pernus, F. and Likar, B., 2010. "A survey of mobile robots for distribution power line inspection". *IEEE Transactions on Power Delivery*, Vol. 25, No. 1, pp. 485–493.

Luque-Vega, L., Castillo-Toledo, B., Loukianov, A. and González-Jiménez, L., 2014. "Power line inspection via an unmanned aerial system based on the quadrotor helicopter". pp. 393–397. ISBN 978-1-4799-2337-3. doi: 10.1109/MELCON.2014.6820566.

Miller, R., Abbasi, F. and Mohammadpour, J., 2017. "Power line robotic device for overhead line inspection and maintenance". *Industrial Robot*, Vol. 44, No. 1, pp. 75–84.

Parker, L.E. and Draper, J.V., 1998. "Robotics applications in maintenance and repair". *Handbook of industrial robotics*, Vol. 2, pp. 1023–1036.

Toussaint, K., Pouliot, N. and Montambault, S., 2009. "Transmission line maintenance robots capable of crossing obstacles: state-of-the-art review and challenges ahead". *Journal of Field Robotics*, Vol. 26, No. 5, pp. 477–499.

Wang, L., Liu, F., Xu, S., Wang, Z., Cheng, S. and Zhang, J., 2010. "Design, modeling and control of a biped line-walking robot". *International Journal of Advanced Robotic Systems*, Vol. 7, No. 4, p. 33. doi:10.5772/10498. URL `https://doi.org/10.5772/10498`.

9. RESPONSIBILITY NOTICE

The authors are solely responsible for the printed material included in this paper.